Supporting Information

Efficient polyethylene terephthalate biodegradation by an engineered *Ideonella sakaiensis* PETase with a fixed substrate binding W156 residue

Qingdian Yin, [†a] Jiaxing Zhang, [†a] Sen Ma, [†e] Tao Gu, [a] Mengfan Wang, [e] Shengping You, [*ad] Sheng Ye, [*e] Rongxin Su, [abcd] Yaxin Wang [*e] and Wei Qi [*abcd]

* Corresponding author.

† These authors contributed equally to this work.

Addresses:

[a] Chemical Engineering Research Center, School of Chemical Engineering and Technology, Tianjin University, Tianjin 300350, PR China

[b] State Key Laboratory of Chemical Engineering, Tianjin University, Tianjin 300350, PR China

[c] Collaborative Innovation Center of Chemical Science and Engineering (Tianjin), Tianjin 300072, PR. China

[d] Tianjin Key Laboratory of Membrane Science and Desalination Technology, Tianjin University, Tianjin 300072, PR China

[e] Tianjin Key Laboratory of Function and Application of Biological Macromolecular Structures, School of Life Sciences, Tianjin University, 92 Weijin Road, Nankai District, Tianjin 300072, P.R. China.

Tel: +86 22 27407799

Fax: +86 22 27407599

E-mail address: ysp@tju.edu.cn (Shengping You); sye@tju.edu.cn (Sheng Ye); wangyaxin@tju.edu.cn (Yaxin Wang); qiwei@tju.edu.cn (Wei Qi)

Contents

1. Supporting Figures

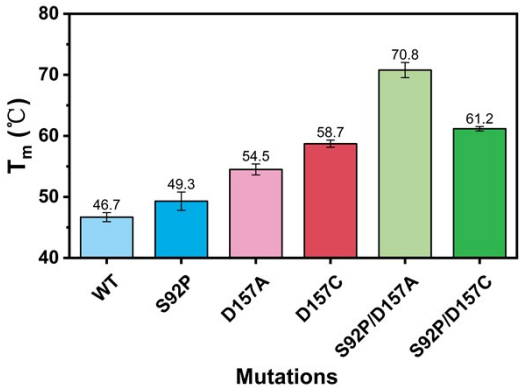

Figure S1. T_m values of *Is*PETase^{WT} and variants.

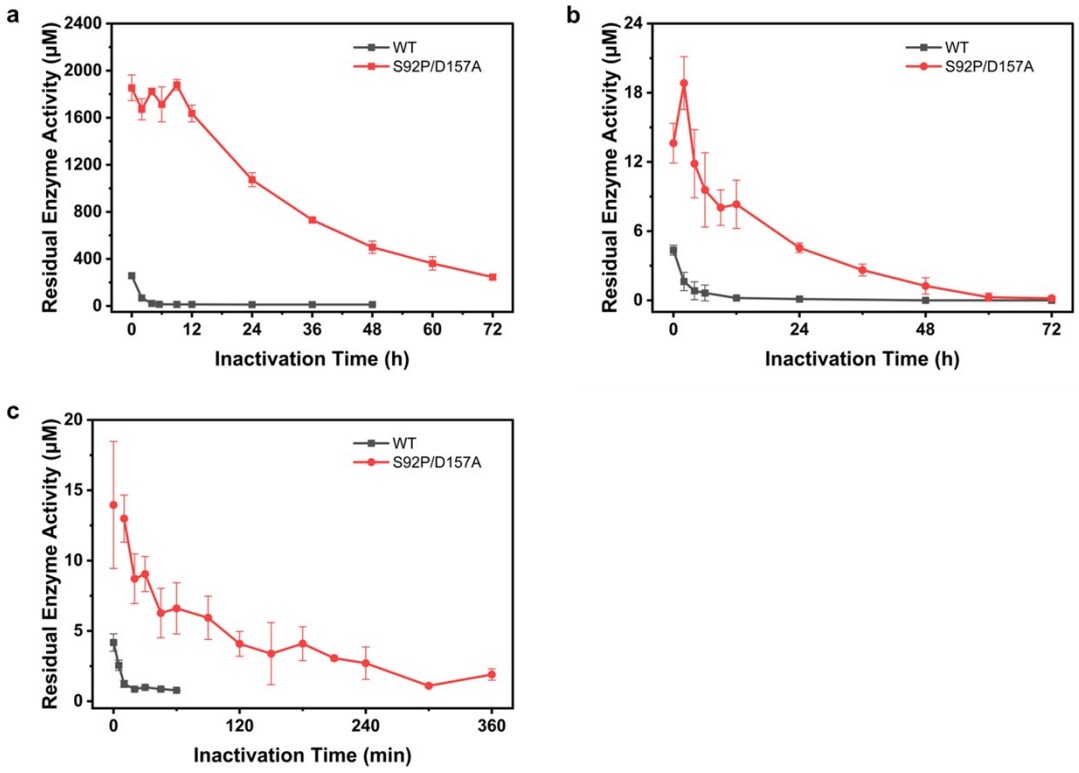

Figure S2. The durability of *Is*PETase^{WT} and the S92P/D157A variant. (a) Inactivation at 40 °C and then incubated with amPET at 40 °C for 12 h. (b) Inactivation at 40 °C and then incubated with hcPET at 40 °C for 24 h. (c) Inactivation at 50 °C and then incubated with hcPET at 40 °C for 24 h. The reaction mixture (500 nM *Is*PETase in 300 μL of glycine-NaOH (pH 9.0, 50 mM) buffer) was inactivated at 40 °C or 50 °C for different duration. Next, the reaction mixture was cooled on ice for 5 minutes. Then the PET films (ø=6 mm) were soaked in inactivated reaction mixtures and incubated at 40 °C for 12 h (amPET) or 24 h (hcPET). After removing the PET film from the reaction mixture, the enzyme reaction was terminated by heating at 85 °C for 15 min. Residue enzyme activity was evaluated by measuring the amount of PET monomers (the sum of TPA, MHET, and BHET) released by HPLC.

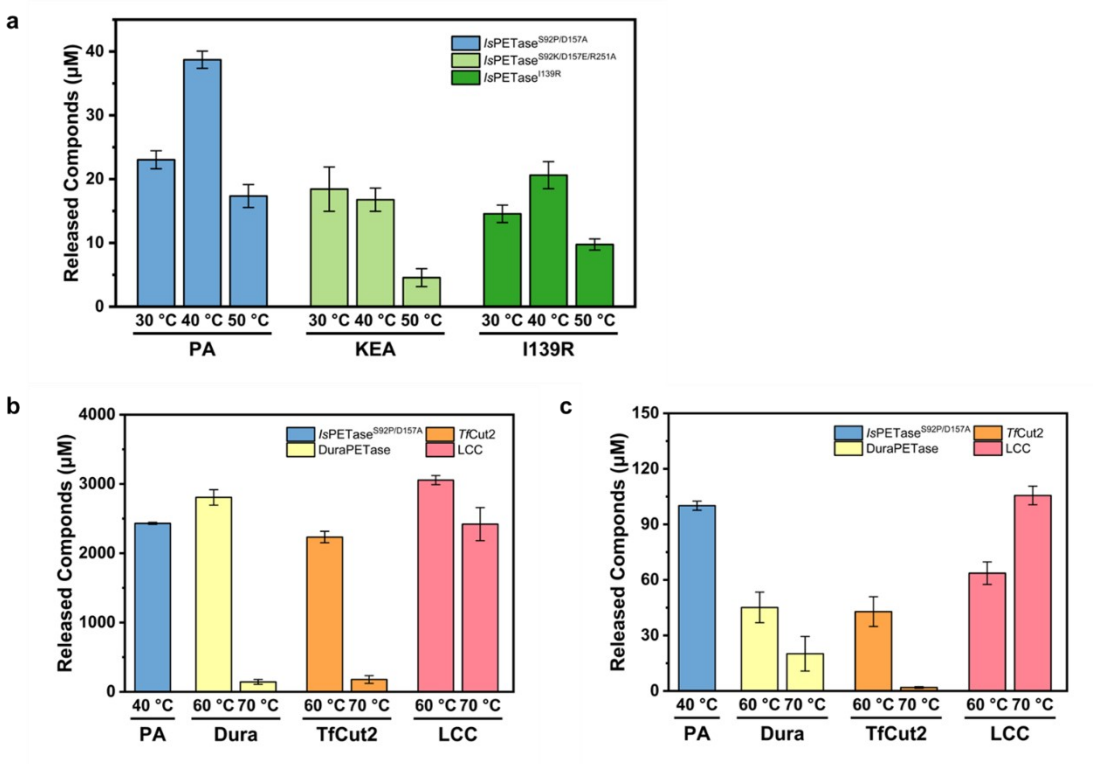

Figure S3. Comparison of degradation activity of the S92P/D157A variant and variants constructed in our previous research (a). Comparison of degradation activity of the S92P/D157A variant and thermostable homologous PET hydrolases towards amPET (b) and hcPET (c). The PET films (ø=6 mm) were soaked in 300 μL of glycine-NaOH (pH 9.0, 50 mM) buffer with 500 nM enzyme under reaction temperatures indicated in the figure for 24 h. PET degradation activity was evaluated by measuring the amount of PET monomers (the sum of TPA, MHET, and BHET) released. All measurements were conducted in triplicate (n=3).

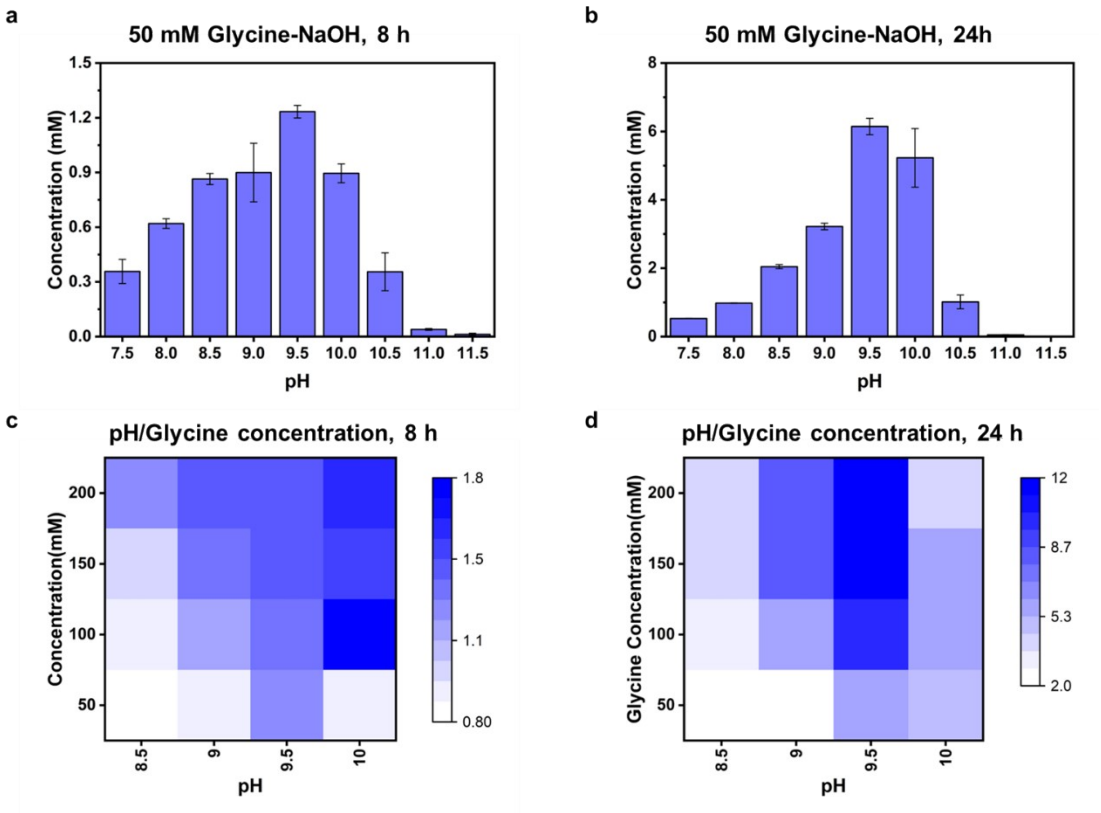

Figure S4. Optimization of glycine concentration and pH of the reaction condition. The amPET films (ø=6 mm) were soaked in 300 µL of 50 mM glycine-NaOH buffer with 500 nM enzyme under pH conditions ranging from 7.5 to 11.5 first (a, b). The pH gradient was narrowed to 8.5-10.0 and further tested for different glycine concentrations ranging from 50 to 200 mM (c, d). After removing the PET film from the reaction mixture, the enzyme reaction was terminated by heating at 85 °C for 15 min. The amount of PET monomers (the sum of TPA, MHET, and BHET) released was analyzed by HPLC. All measurements were conducted in triplicate (n=3).

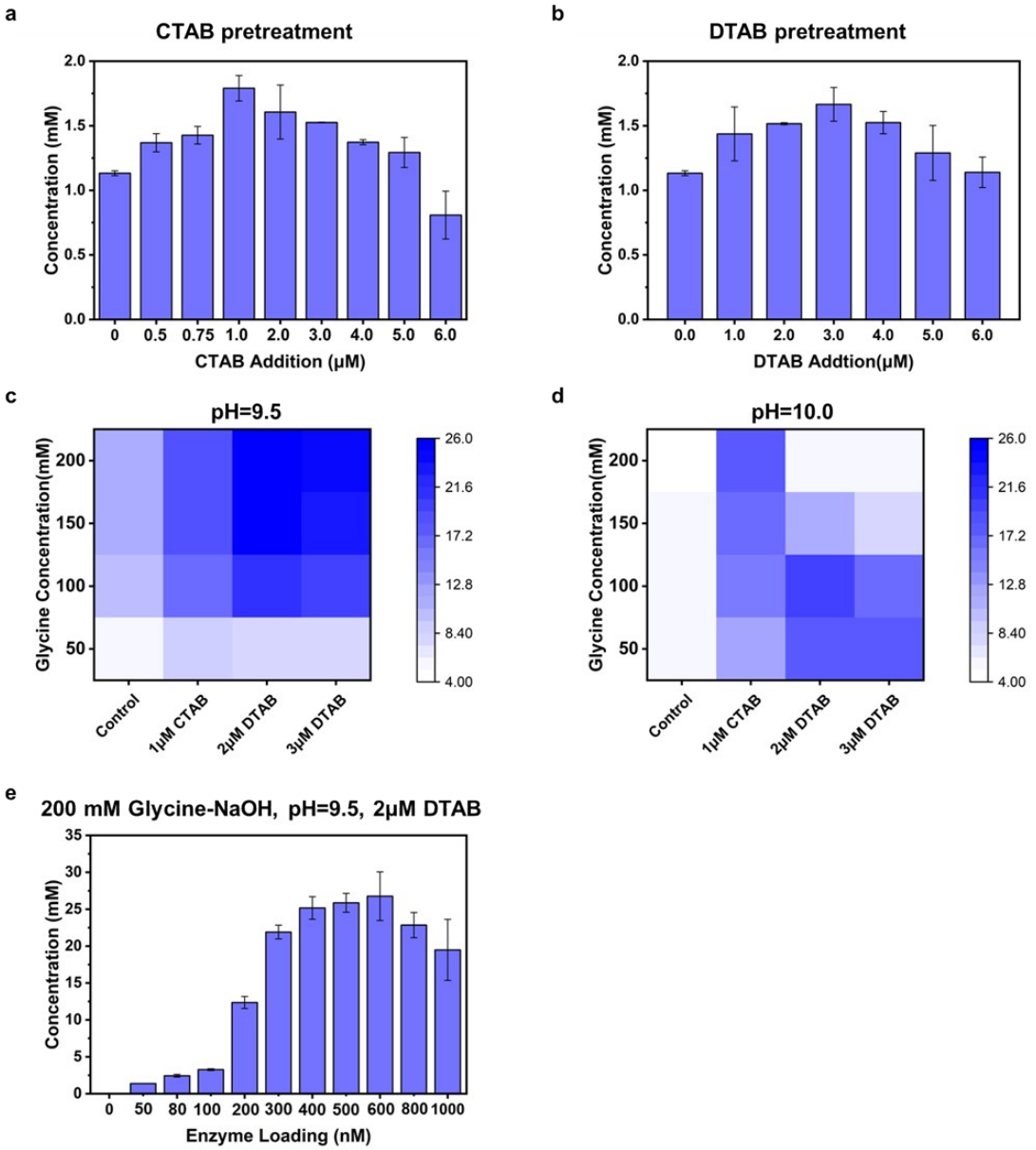

Figure S5. Optimization of surfactant addition and enzyme loading. Different dosages of CTAB and DTAB pretreatment were tested first with the amPET films (ø=6 mm) soaking in 300 μL of glycine-NaOH buffer (50 mM, pH=9.0) and supplemented with 500 nM enzyme (a, b). Next, the optimal surfactant pretreatment conditions and their compatibility with buffer conditions were tested (c, d). Last, different enzyme loadings were tested under reaction conditions of 200 mM glycine-NaOH, pH=9.5, 2 μM DTAB pretreatment (e). The amount of PET monomers (the sum of TPA, MHET, and BHET) released was analyzed by HPLC.

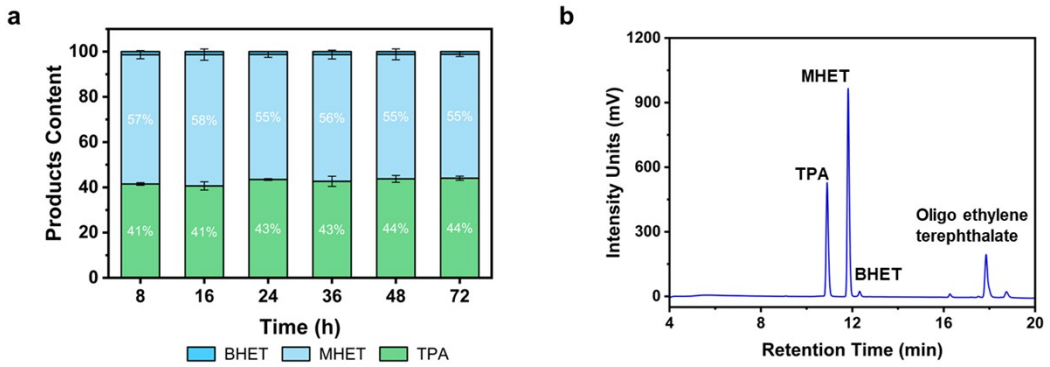

Figure S6. (a) Soluble monomer ratio changes in the depolymerization process of S92P/D157A variant towards amPET. (b) Representative HPLC result of product released in the amPET depolymerization process.

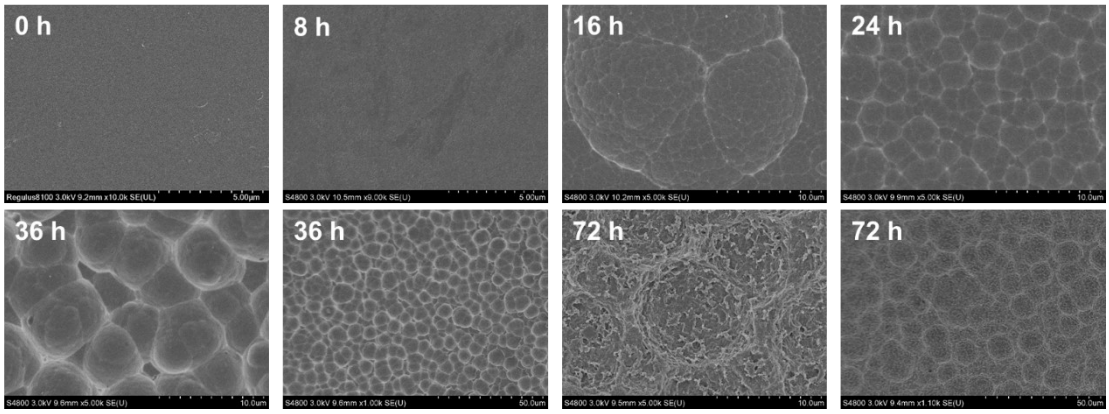

Figure S7. SEM images of amPET films following various exposure times with the S92P/D157A variant.

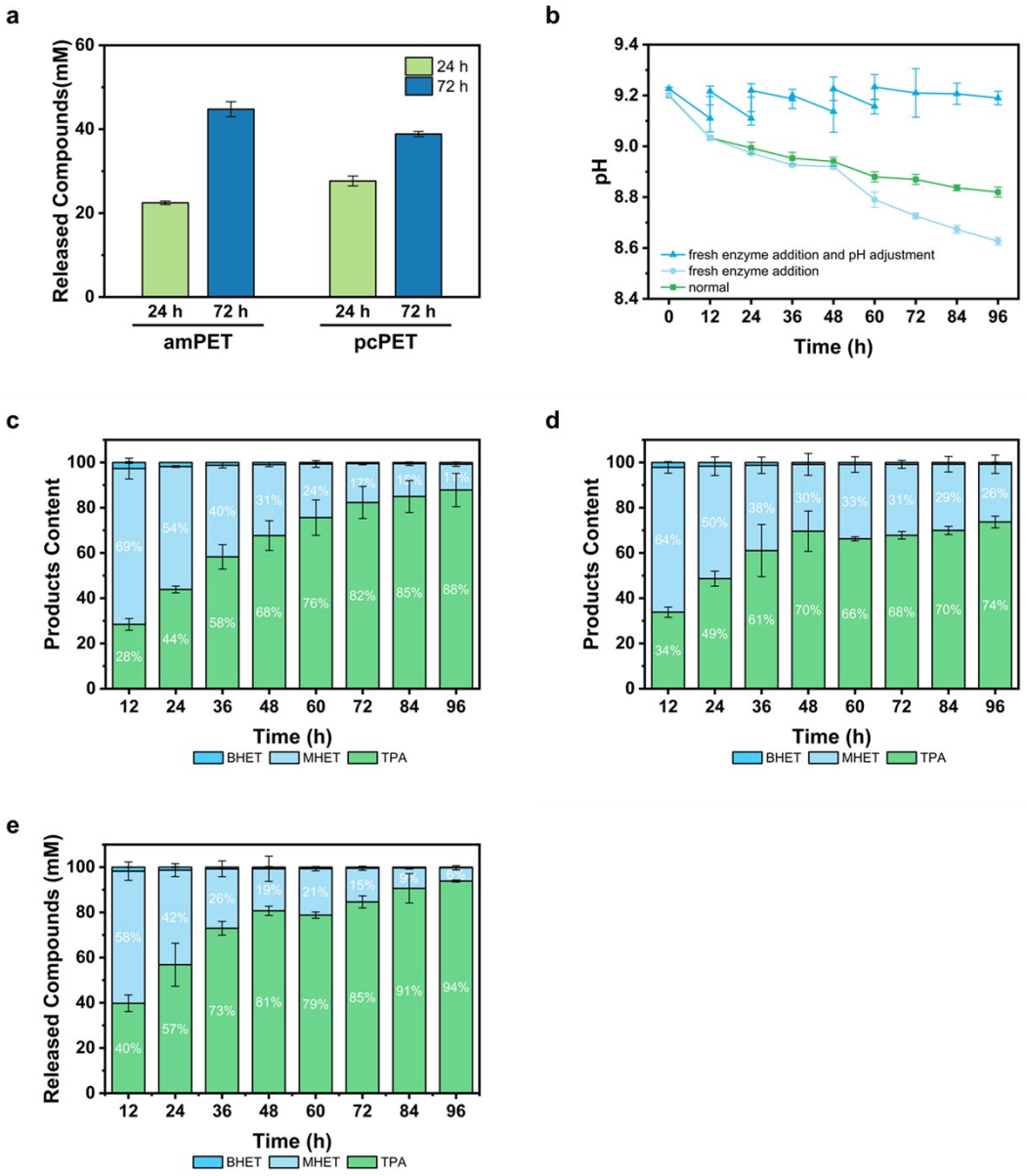

Figure S8. (a) Comparison of depolymerization degree of amPET and pcPET. The PET films (ø=6 mm) were soaked in 200 mM glycine-NaOH, pH=9.5 with 2 μM DTAB pretreatment and 600 nM enzyme loading. (b) The pH change in the pcPET depolymerization process. Soluble monomer ratio change in the pcPET depolymerization process under different conditions: (c) normal; (d) with fresh enzyme addition; and (e) with fresh enzyme addition and pH adjustment.

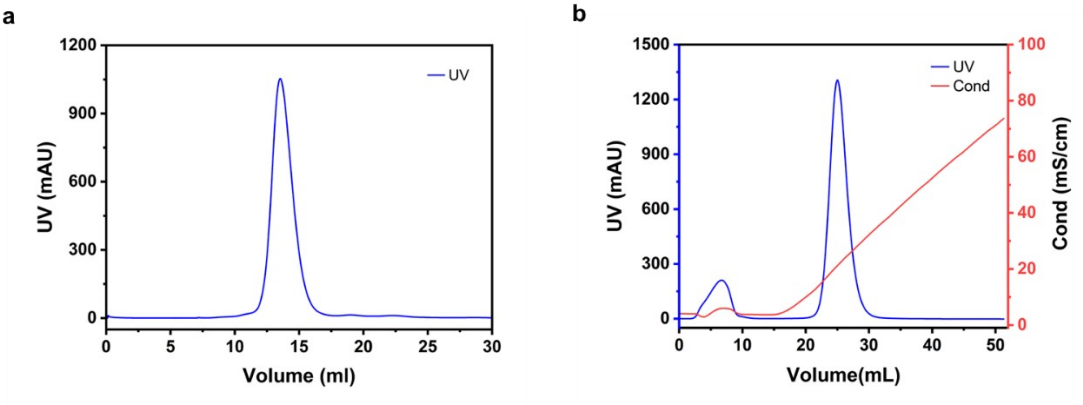

Figure S9. Size-exclusion chromatography (a) and ion exchange chromatography (b) analyses of the S92P/D157A variant.

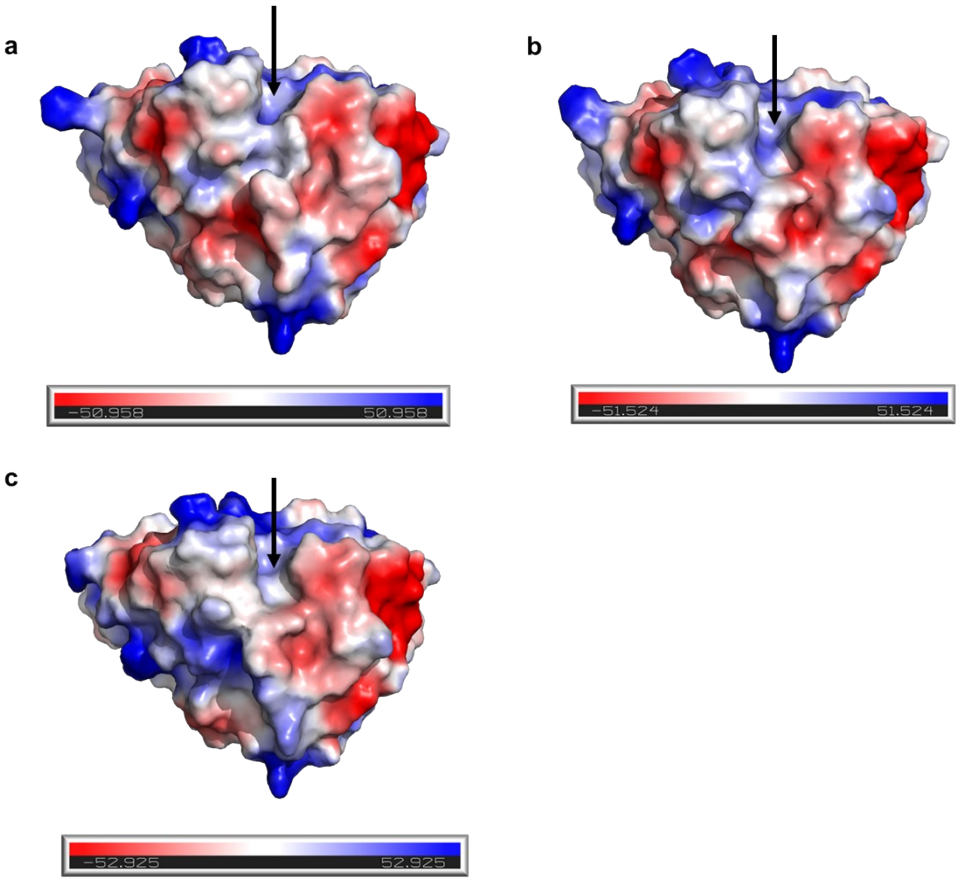

Figure S10. Plot of molecular electrostatic potential (MESP) for *Is*PETase^{WT} chain A (a), *Is*PETase^{WT} chain B (b), and the S92P/D157A variant chain A (c). The active site is highlighted with an arrow.

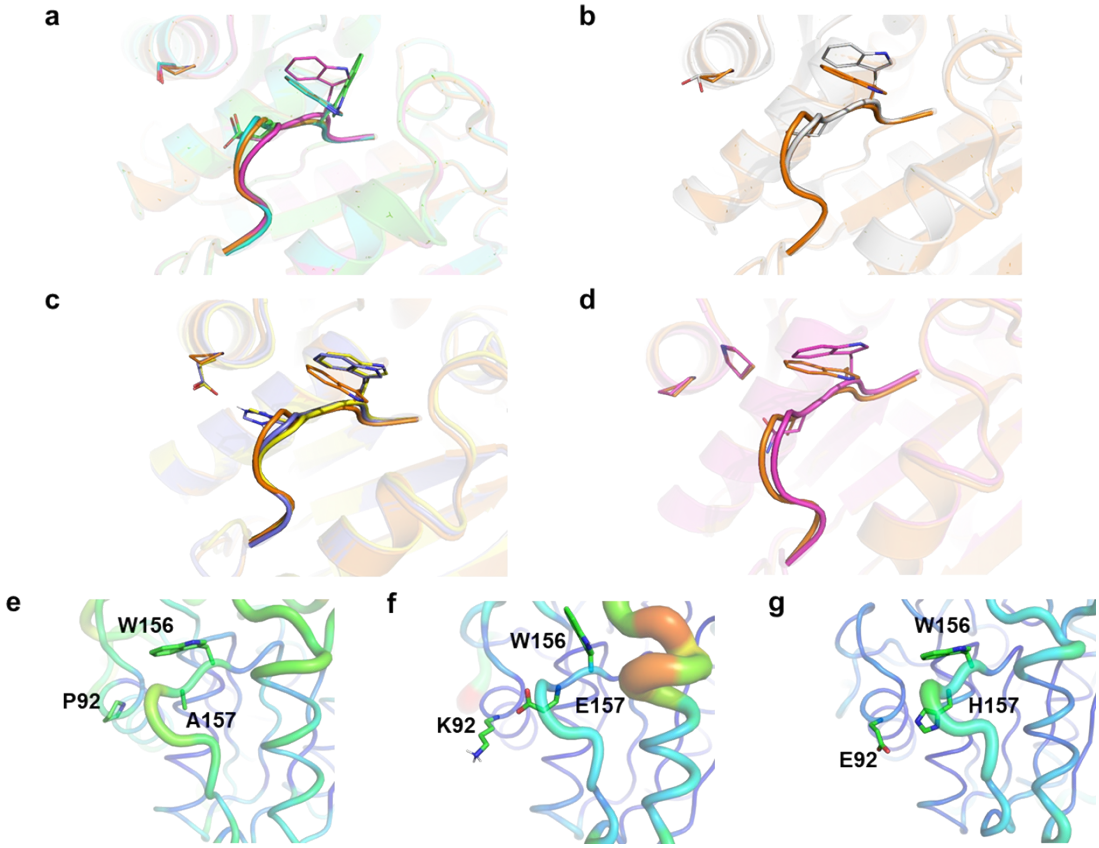

Figure S11. Stereo view of the substrate-binding W156 and β6-β7 loop nearby region. (a) Align S92P/D157A chain A (orange) with *Is*PETase^{WT} chain A (green), B (cyan), and C (magenta). (b) Align S92P/D157A chain A (orange) with *Is*PETase^{S185H} (PDB 7CY0, grey). The residues P92, A157, and W156 in the S92P/D157A variant and the residues S92, D157, and W156 in *Is*PETase^{WT} and *Is*PETase^{S185H} were shown as sticks. (c) Align S92P/D157A chain A with *Tf*Cut2 (PDB 4CG1, slate) and LCC (PDB 4EB0, yellow). The corresponding residues D94, H156, and W155 in *Tf*Cut2, and residues D129, H191, and W190 in LCC were shown as sticks. (d) Align S92P/D157A chain A (orange) with *Bur*PL (PDB 7CWQ, magenta). The corresponding residues P248, P249, N316, and W315 in *Bur*PL were shown as sticks. B-factors of the structures and residues related to the β6-β7 connecting loop stabilization in the S92P/D157A variant (e), the *Is*PETase$^{S92K/D157E/R251A}$ variant (f) and ThermoPETase (PDB 6IJ6) (g).

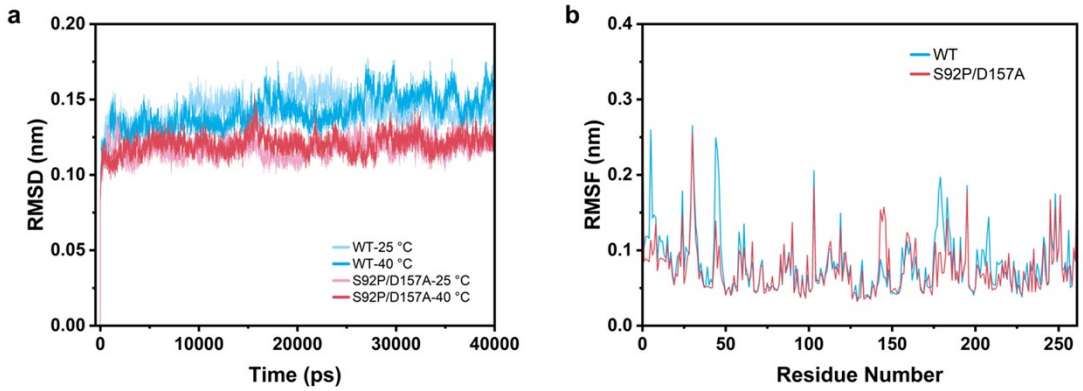

Figure S12. Analysis of free enzymes by MD simulation. (a) Root mean square deviation (RMSD) of the Cα atoms of *Is*PETase^{WT} and the S92P/D157A variant. (b) Root mean square fluctuation (RMSF) of the Cα atoms per residue of *Is*PETase^{WT} and the S92P/D157A variant at 40 °C.

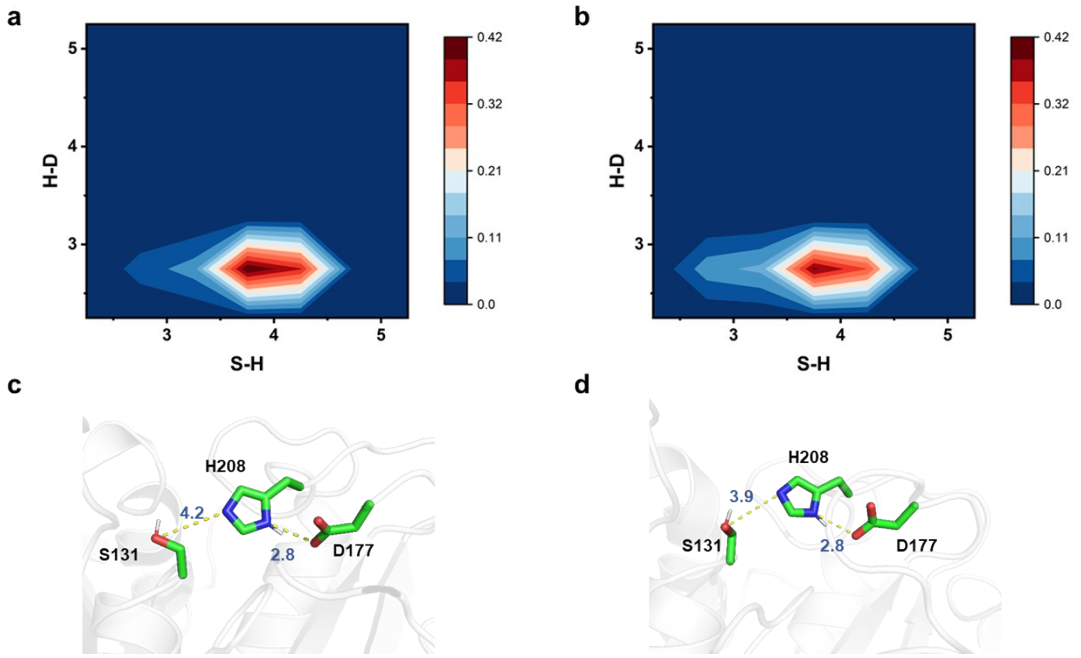

Figure S13. Catalytic triad distance distribution in *Is*PETase^{WT} and the S92P/D157A variant. From 5 replicates, totaling 200 ns of MD simulations, the distance between S131-H208 and H208-D177 was plotted as the probability density of the figure. The conformation with the highest probability density obtained by clustering was represented with a 3D model. The catalytic triads (S131-H208-D177) are shown as sticks and colored by elements of carbon (green), nitrogen (blue), and oxygen (red). Yellow colored dashed line indicates the heavy-atom distance in Å between residues.

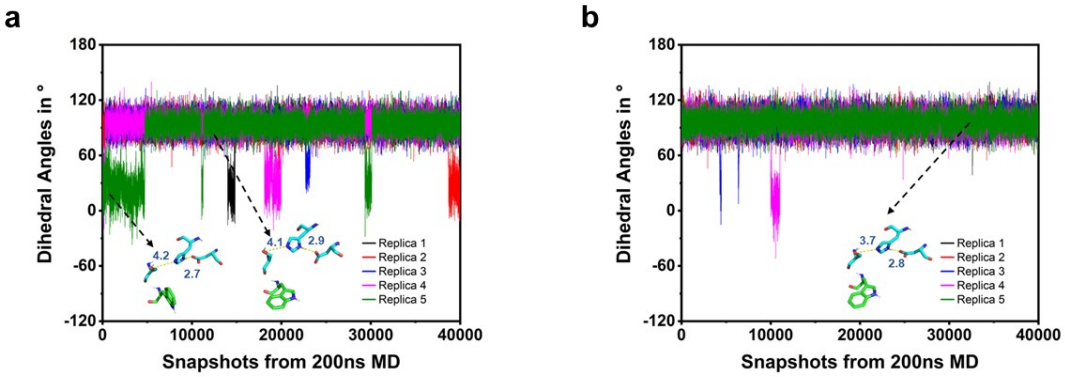

Figure S14. W156 sidechain conformational variations in *Is*PETase^{WT} and the S92P/D157A variant. From 5 replicates, totaling 200 ns of MD simulation, the dihedral angle between C_α-C_β-C_γ-$C_{\delta1}$ atoms in W156 was retrieved and plotted as shown in the figure. Side-chain conformations are defined as different when any of the χ dihedral angles changes >30°. The prominent clusters of W156 sidechains were also represented with a 3D model. The catalytic triads (S131-D177-H208) are shown as cyan sticks and the W156 residue is shown as green sticks. The distances between the catalytic residues are shown as dotted lines and are in Å.

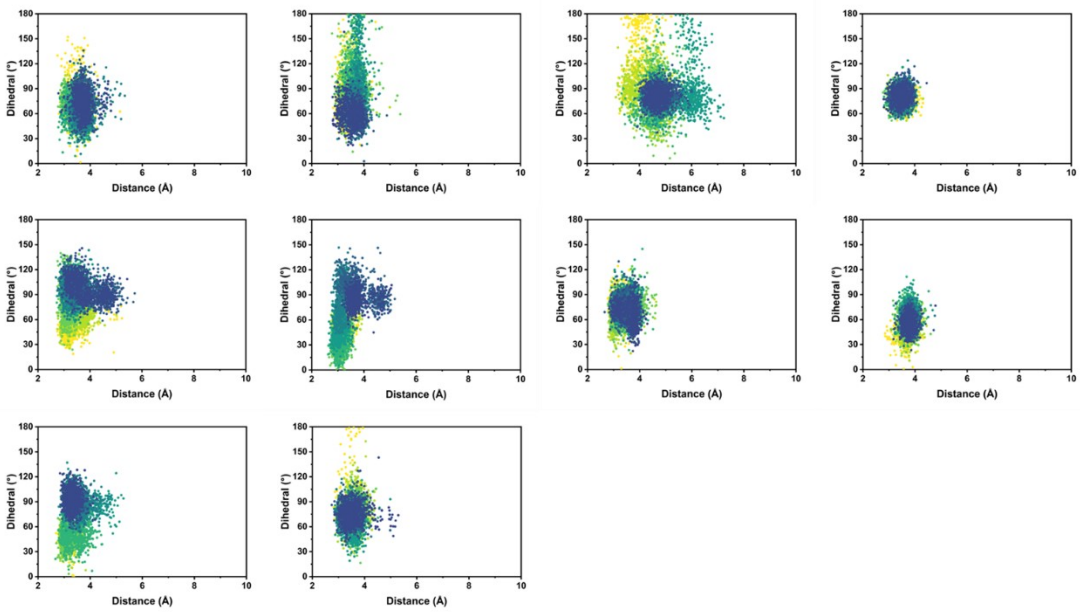

Figure S15. Catalytic distance (the Oγ of S131 and the carbonyl carbon of 2PET) change and scissile ethylene glycol conformational variations (OC-CO torsion angle Ψ) of *Is*PETase^{WT} in the MD simulations. The ten highest-scoring docking poses were subjected to 5 ns MD simulations, respectively. The time variation from 0 to 5 ns is indicated by the color change from yellow to blue.

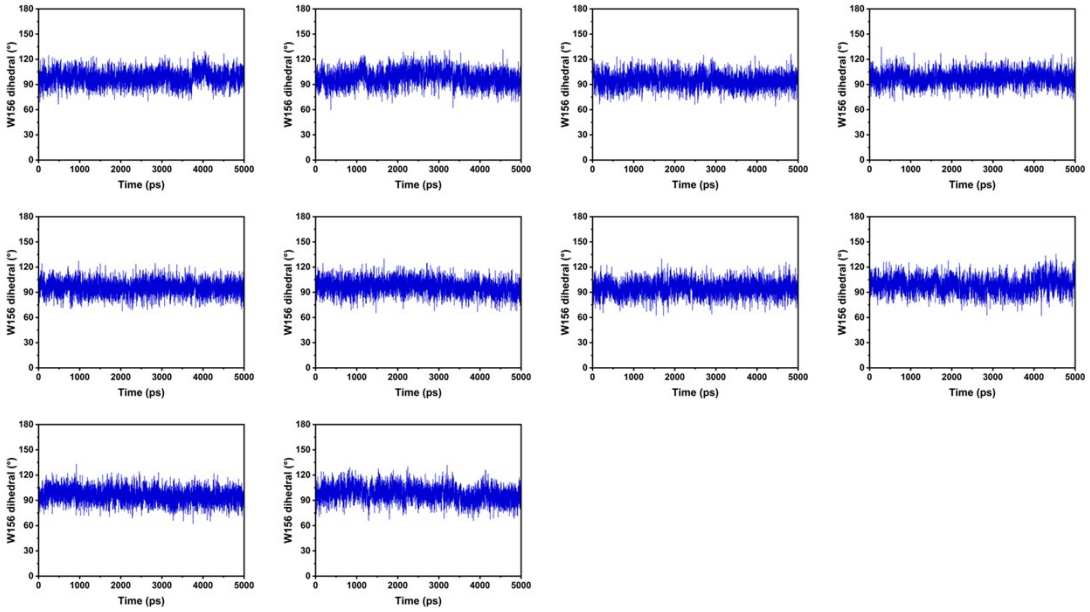

Figure S16. W156 conformational variations (dihedral angle between C_{α}-C_{β}-C_{γ}-$C_{\delta 1}$ atoms in W156) versus time in the MD simulations of *Is*PETase^{WT}.

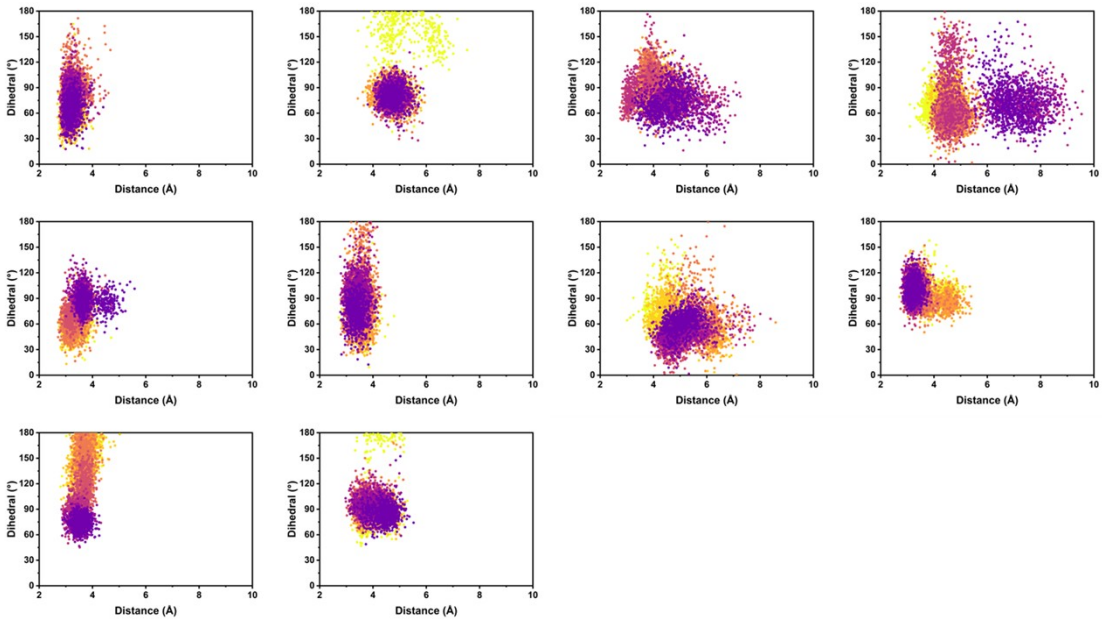

Figure S17. Catalytic distance (the Oγ of S131 and the carbonyl carbon of 2PET) change and scissile ethylene glycol conformational variations (OC-CO torsion angle Ψ) of the S92P/D157A variant in the MD simulations. The ten highest-scoring docking poses were subjected to 5 ns MD simulations, respectively. The time variation from 0 to 5 ns is indicated by the color change from yellow to purple.

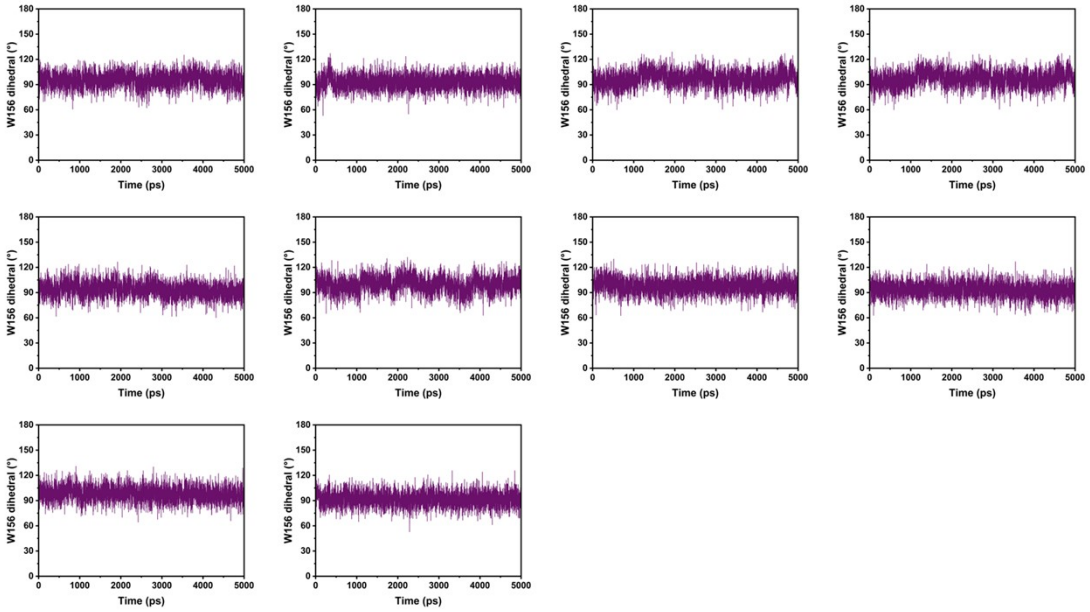

Figure S18. W156 conformational variations (dihedral angle between C_α-C_β-C_γ-$C_{\delta1}$ atoms in W156) versus time in the MD simulations of the PA variant.

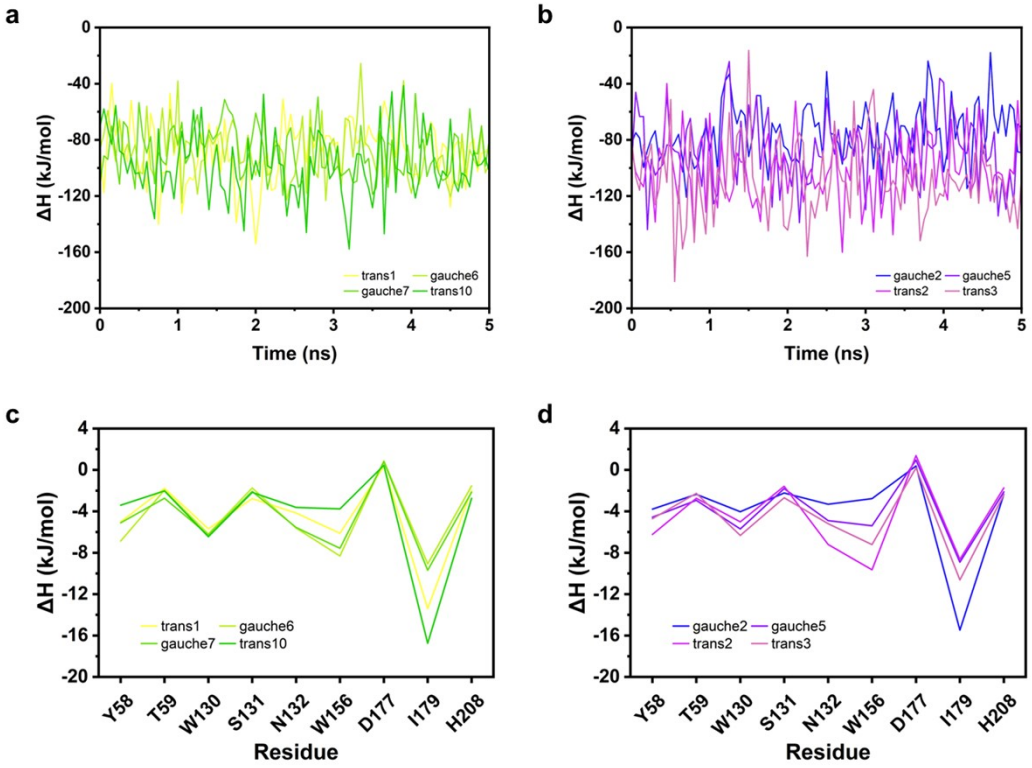

Figure S19. Binding energy of enzyme/substrate complex. The binding energy variation of 2PET/*Is*PETase^{WT} complex (a) and 2PET/PA variant complex (b)versus time. The average pairwise energy contribution of residues in *Is*PETase^{WT} (c) and the PA variant (d) towards the substrate.

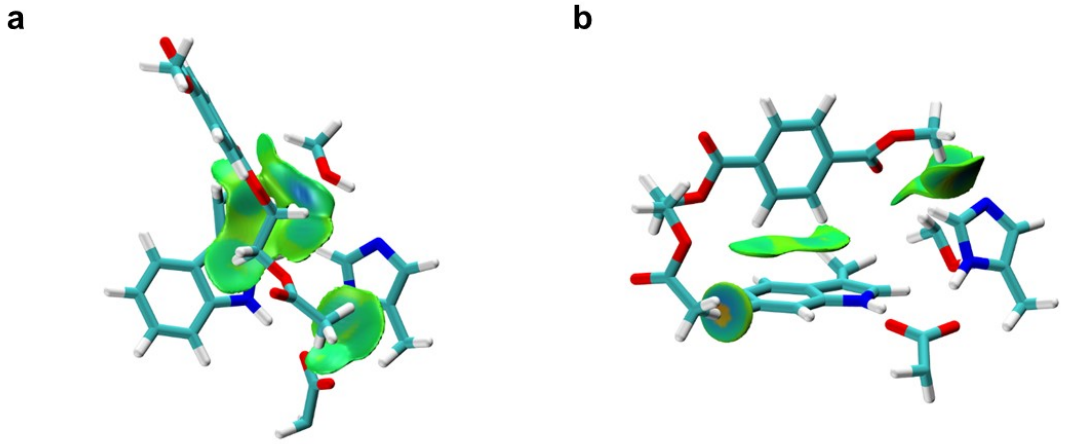

Figure S20. Interactions between W156 residue with the substrate. (a) Weak hydrophobic C-H···π between W156 with the backbone of the EG unit. (b) T-stacking interaction between W156 with the phenyl ring of PET substrate.

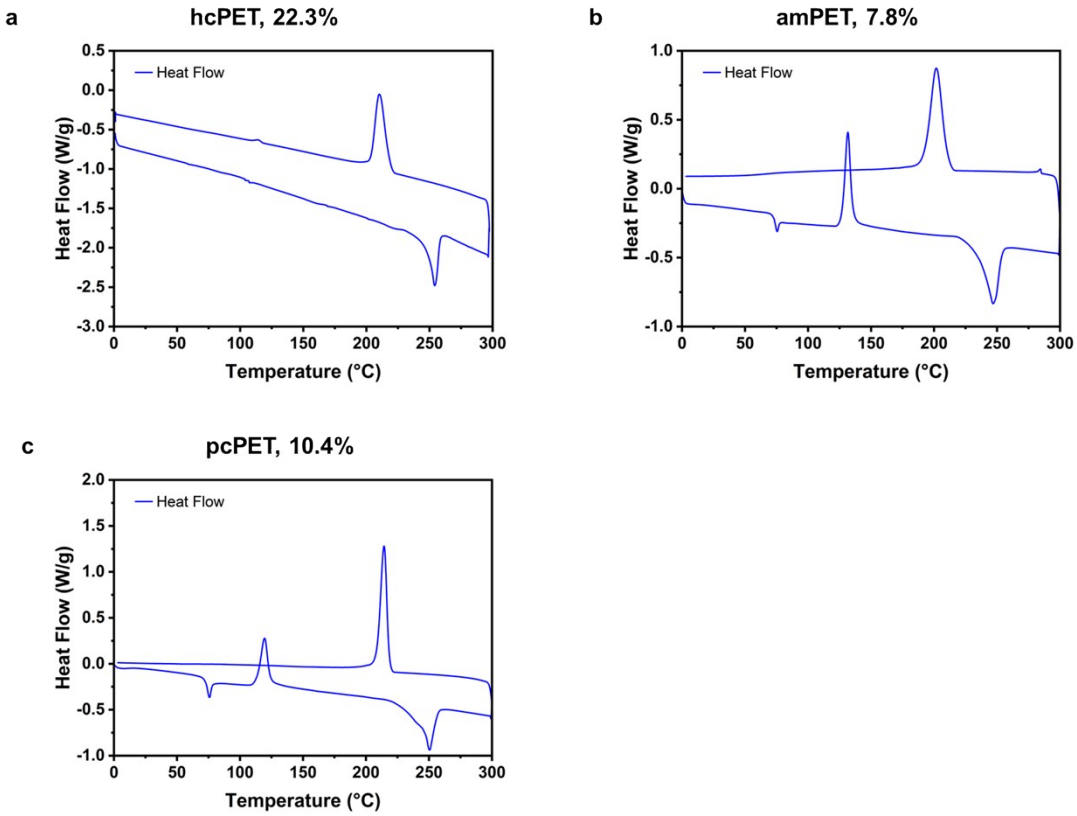

Figure S21. Differential scanning calorimetry (DSC) for determining the crystallinity of PET films.

2. Supporting Tables

Table S1. Primers used for site-directed mutagenesis.

Name	Primer (5'-3')
S92K-F	cgaccagccgAAAagccgctcgtcgcagcagatgg
S92K-R	cgagcggctTTTcggctggtcgagcgtggagttggtg
S92R-F	cacgctcgaccagccgCGcagccgctcgtcg
S92R-R	CGcggctggtcgagcgtggagttggtgtc
S92P-F	ccacgctcgaccagccgCccagccgctcgtcg
S92P-R	Gcggctggtcgagcgtggagttggtgtc
S92I-F	ccacgctcgaccagccgATcagccgctcgtcg
S92I-R	ATcggctggtcgagcgtggagttggtgtc
S92G-F	ccacgctcgaccagccgGGcagccgctcgtcg
S92G-R	CCcggctggtcgagcgtggagttggtgtc
S92C-F	ccacgctcgaccagccgtGTagccgctcgtcgc
S92C-R	ACcggctggtcgagcgtggagttggtgtc
S92N-F	ccacgctcgaccagccgAAcagccgctcgtcg
S92N-R	TTcggctggtcgagcgtggagttggtgtc
S92F-F	cacgctcgaccagccgtTcagccgctcgtcg
S92F-R	Aacggctggtcgagcgtggagttggtgtc
S92W-F	cacgctcgaccagccgtGGagccgctcgtcg
S92W-R	CCacggctggtcgagcgtggagttggtgtc
D157H-F	gccgcaggccccgtggCacagctcgaccaac
D157H-R	Gccacggggcctgcggcgccgcggctttc
D157E-F	ccgcaggccccgtgggaGagctcgaccaac
D157E-R	Ctcccacggggcctgcggcgccgcggctttc
D157A-F	cgcaggccccgtgggCGagctcgaccaacttc
D157A-R	CGcccacggggcctgcggcgccgcggctttc
D157V-F	cgcaggccccgtgggTGagctcgaccaacttc
D157V-R	CAcccacggggcctgcggcgccgcggctttc
D157I-F	gccgcaggccccgtggATcagctcgaccaac
D157I-R	ATccacggggcctgcggcgccgcggctttc
D157L-F	gccgcaggccccgtggCTcagctcgaccaac
D157L-R	AGccacggggcctgcggcgccgcggctttc

D157G-F	cgcaggccccgtgggGCagctcgaccaacttc
D157G-R	GCcccacggggcctgcggcgccgcggctttc
D157C-F	cgccgcaggccccgtggTGcagctcgaccaac
D157C-R	CAccacggggcctgcggcgccgcggctttc
D157N-F	gccgcaggccccgtggAacagctcgaccaac
D157N-R	Tccacggggcctgcggcgccgcggctttc
D157S-F	cgcaggccccgtggAGcagctcgaccaacttc
D157S-R	CTccacggggcctgcggcgccgcggctttc
D157T-F	cgcaggccccgtggACcagctcgaccaacttc
D157T-R	GTccacggggcctgcggcgccgcggctttc
D157F-F	gccgcaggccccgtggTTcagctcgaccaac
D157F-R	AAccacggggcctgcggcgccgcggctttc
D157W-F	ccgcaggccccgtggTGGagctcgaccaacttc
D157W-R	CCAcccacggggcctgcggcgccgcggctttc
D157Y-F	gccgcaggccccgtggTacagctcgaccaac
D157Y-R	Accacggggcctgcggcgccgcggctttc

Table S2. Data collection and refinement statistics of *Is*PETase$^{S92P/D157A}$.

Parameters	***Is*PETase$^{S92P/D157A}$**
X-ray Source	BL10U2
Wavelength (Å)	0.97918
Space group	$C222_1$
Unit cell parameters (Å)	a=52.6, b=233.8, c=163.7
Resolution range (Å)	58.45-1.97 (2.02-1.97)*
Unique reflections	71,765 (5,267)
Completeness (%)	99.8 (99.5)
Redundancy	11.4 (7.9)
I/σ(I)	14.7 (2.0)
R_{merge} (%)	10.1 (14.7)
R_{meas} (%)	10.6 (15.7)
R_{pim} (%)	3.1 (5.5)
$CC_{1/2}$	0.998 (0.672)
Refinement statistics	
Resolution range (Å)	37.91-1.97 (2.04-1.97)
Reflections used in refinement	71,704 (7,070)
Reflections used for R-free	3,529 (362)
R_{work} (%)	17.6 (31.0)
R_{free} (%)	21.3 (33.9)
Number of non-hydrogen atoms	6,531
Protein	5,770
Solvent	761
Average B-factors	43.9
Protein	42.8
Solvent	52.0
r.m.s. deviations	
Bond lengths (Å)	0.007
Bond angles (°)	0.82
Ramachandran	
Favored (%)	98.5
Allowed (%)	1.5
Outliers (%)	0.0

*Numbers in the brackets are for the highest resolution shell.

Table S3. Substrate docking and conformation change of *Is*PETase^{WT} in MD simulation.

WT	Docking Score	RMSD (Å)	Start Conformation	End Conformation	Notes
1	56.1164	0.826	*trans*	*gauche*	
2	54.5609	0.835	*trans*	*gauche*	
3	54.5609	0.749	*trans*	*gauche*	
4	53.6003	0.702	*gauche*	*gauche*	
5	53.5392	0.858	*gauche*	*gauche*	
6	53.4832	0.855	*gauche*	*gauche*	
7	53.3957	0.920	*gauche*	*gauche*	
8	53.3957	0.860	*gauche*	*gauche*	
9	52.5788	0.892	*gauche*	*gauche*	
10	52.2403	0.902	*trans*	*gauche*	

Table S4. Substrate docking and conformation change of the PA variant in MD simulation.

PA	Docking Score	RMSD (Å)	Start Conformation	End Conformation	Notes
1	49.5914	0.734	*trans*	*gauche*	
2	48.0079	0.838	*trans*	*gauche*	
3	46.7246	0.751	*gauche*	*gauche*	
4	46.582	0.780	*gauche*	*gauche*	Lost productive conformation
5	46.4753	0.662	*gauche*	*gauche*	
6	46.1443	0.695	*gauche*	*gauche*	
7	46.0372	0.677	*gauche*	*gauche*	Lost productive conformation
8	45.8445	0.694	*gauche*	*trans*	
9	45.7686	0.802	*trans*	*gauche*	
10	45.6075	0.685	*gauche*	*gauche*	

Table S5. Binding energy calculation of enzyme/substrate complex.

	5XG0					PA				
Replica	Average of the 4 replica	1	6	7	10	Average of the 4 replica	3	6	8	9
Conformation Change	-	*Trans-gauche*	*Gauche-gauche*	*Gauche-gauche*	*Trans-gauche*	-	*Gauche-gauche*	*Gauche-gauche*	*Trans-gauche*	*Trans-gauche*
Y58	-5.1	-5.0	-6.9	-5.1	-3.4	-4.8	-3.8	-4.6	-6.2	-4.7
T59	-2.1	-1.8	-2.0	-2.7	-2.0	-2.6	-2.4	-2.9	-2.7	-2.3
W130	-6.2	-5.7	-6.2	-6.3	-6.5	-5.3	-4.0	-5.7	-5.0	-6.3
S131	-2.2	-2.8	-1.7	-2.1	-2.2	-2.1	-2.2	-1.8	-1.6	-2.7
N132	-4.7	-4.2	-5.6	-5.6	-3.6	-5.2	-3.3	-4.9	-7.2	-5.2
W156	-6.4	-6.1	-8.3	-7.6	-3.8	-6.3	-2.8	-5.4	-9.6	-7.2
D177	0.6	0.3	0.9	0.8	0.4	0.7	0.4	1.0	1.4	0.2
I179	-12.2	-13.4	-9.1	-9.7	-16.7	-10.9	-15.5	-8.9	-8.6	-10.6
H208	-2.1	-2.0	-1.5	-2.1	-2.7	-2.1	-2.4	-2.1	-1.7	-2.4
The sum of key residues	-40.5	-40.6	-40.5	-40.4	-40.5	-38.5	-36.0	-35.4	-41.4	-41.2
5 ns Average	-90.9	-88.1	-88.3	-89.0	-98.3	-92.9	-74.3	-87.2	-101.9	-108.1
Last 0.5 ns Average	-93.1	-89.2	-95.5	-84.9	-102.9	-96.0	-65.7	-100.2	-101.7	-116.4

3. Materials and methods

3.1 Semi-saturation mutagenesis

The gene encoding all proteins used in this study was chemically synthesized (GENEWIZ, Suzhou, China) and cloned to the pET22b vector for recombinant protein expression in *Escherichia coli*. Variants were constructed by using a *Fast* Mutagenesis System (TransGen, Beijing, China) with the wild-type *Is*PETase plasmid as a template. The primers are provided in Table S1.

3.2 Protein expression and purification

The pET22b-*Is*PETase plasmid, either wild type, variants, or DuraPETase, was transformed into *E. coli* strain BL21 (DE3) cells that were grown in LB medium at 37 °C to an OD_{600} of 0.8 - 1.0 and then induced by the addition of 0.5 mM isopropyl β-D-1-thiogalactopyranoside (IPTG) at 16 °C for 16 h. Cells were harvested by centrifugation at 4,000 rpm for 10 min and then resuspended in buffer A (25 mM Tris-HCl, 150 mM NaCl, pH 7.5) and then disrupted by high-pressure homogenization. Cell debris was removed by centrifugation at 16,000 rpm for 1 h. The supernatant was then applied to a Ni-NTA Sepharose resin (Genscript, Nanjing, China). After washing with buffer A containing 20 mM imidazole, the bound proteins were eluted with 300 mM imidazole in buffer A. For further thermostability and activity tests, the purified protein was concentrated to 10 mg mL^{-1} in buffer B (50 mM Na_2HPO_4-HCl, 100 mM NaCl, pH 7.0). For crystallization screening, the protein was purified by gel filtration on a Superdex 75 HR column equilibrated with buffer A and Capto HiRes S column, concentrated to 30 mg mL^{-1}, flash-frozen in liquid N_2 and stored at -80 °C. All

purification processes were operated at 4 °C. The purity of the obtained proteins was checked by sodium dodecyl sulfate-polyacrylamide gel electrophoresis (SDS-PAGE) analysis and the concentrations were determined with BCA Protein Assay Kit (Solarbio, Beijing). For *Tf*Cut2 and LCC, the protein expression and purification followed the same procedure as that of *Is*PETase, while the purified protein was concentrated to 10 mg mL^{-1} in buffer containing 25 mM Tris-HCl, 200 mM NaCl, pH 7.5 for further thermostability and activity test.

3.3 Crystallization, data collection, and structure determination

All crystallization experiments were conducted at 16 °C using the sitting-drop vapor-diffusion method. In general, 1 μl of protein-containing solution (30 mg mL^{-1}) was mixed with 1 μl of reservoir solution in 48-well Cryschem plates and equilibrated against 100 μl of the reservoir solution. The optimized crystallization condition for *Is*PETase$^{S92P/D157A}$ was as follows: 100 mM MES-NaOH (pH=6.5), 1.7 M $MgSO_4$. Before data collection, the crystals were soaked in cryoprotectants (mother liquid contains 10-20% 4 M sodium formate). X-ray diffraction data were collected on beamline BL10U2 at the Shanghai Synchrotron Radiation Facility at 100 K and a wavelength of 0.97918 Å. Data integration and scaling were performed using HKL3000. The crystal structure of *Is*PETase$^{S92P/D157A}$ was solved by molecular replacement using the structure of *Is*PETase (PDB ID: 5XG0) [1] as a search model through the PHASER program from the CCP4 package. Model building and refinement were performed using PHENIX (version 1.14) and COOT (version 0.8.9). Data collection and refinement statistics are summarized in Table S2.

3.4 Protein melting temperature (T_m) analysis

Differential scanning fluorimetry (DSF) was used to assess the thermostability of the proteins by determining their melting temperature (T_m). Protein samples were loaded onto a 96-well PCR plate (Roche, Shanghai, China). Loaded volumes per well were as follows: 15 µl of buffer B, 9 µl of the 0.4 mg ml^{-1} protein solution, and 1 µl of the 250× SYPRO Orange diluted solution. The PCR plates were then sealed and spun at 2000 rpm for 1 min at 4.0 °C. Differential scanning fluorimetry melt-curve experiments were conducted using a Light Cyder480 real-time PCR system set on the fluorescence resonance energy transfer channel to use the 465 excitation and 580 emission filters. The samples were heated from 25 °C to 100 °C at the rate of 0.3 °C s^{-1}. A single fluorescence measurement was taken every 0.03 seconds. The T_m was determined from the first derivative curve. T_m values correspond to the average of three measurements.

3.5 In vitro analysis of PET depolymerization performance using PET film

To analyze the depolymerization performance of PET by the PET hydrolases, the Goodfellow PET film with high crystallinity (hcPET, 22.3 % crystallinity) and the amorphous Goodfellow PET film with low crystallinity (amPET, 7.8 % crystallinity) were used as substrates. The Goodfellow PET films were prepared in a circular shape with a diameter of 6 mm for each reaction. The PET film (⌀=6 mm) was soaked in 300 µL of glycine-NaOH (pH 9.0, 50 mM) buffer with 500 nM of the enzyme at the temperatures indicated in the figure for 24 h. After the PET film was removed from the reaction mixture, the enzyme reaction was terminated by heating at 85 °C for 15 min. All experiments were conducted in triplicates.

The time-course analysis of amPET film degradation by the S92P/D157A variant was conducted at 40 °C. The reactions were performed in 300 µl of glycine-NaOH (pH 9.5, 200 mM) buffer with 2 µM DTAB pre-treatment for 1 h. Then 600 nM enzyme was added to start the reaction and terminated at time intervals of 12 h to quantify the total PET monomers released at each time point.

3.6 Depolymerization of untreated pcPET

To compare the extent to which amPET and pcPET can be degraded, the pcPET was first prepared in a circular shape with a diameter of 6 mm and used as the substrate for depolymerization under the same optimized reaction condition as for amPET. For the test in a 500 mL shaking flask, a whole piece of the bottom part of a cake container (approximately 2.2 g) was cut into small rectangular flakes (roughly 1×1 cm^2), and the pcPET flakes were soaked in 0.22 L of glycine-NaOH (pH 9.5, 200 mM) buffer and pretreated by 2 mM DTAB for 1 h. Then 600 nM of purified S92P/D157A variant was added to start the reaction at 40 °C under agitation (160 rpm) in a shaker. The reaction pH was regulated at 9.2 by the addition of 5 M NaOH every 12 h and 600 nM fresh enzyme solution was supplemented after 48 h as required. 250 µL of the reaction mixture was taken at time intervals of 12 h and analyzed by HPLC. The reaction was terminated after 96 h and the PET solids remaining in the solution were separated and air-dried for weighing.

3.7 Analytical method for measuring PET monomers released

The assay samples were filtered with 0.22 µm nylon syringe filters before applying them to high-performance liquid chromatography (HPLC) analysis. All samples were

detected by high-performance liquid chromatography (HPLC, Agilent Technologies 1200 Series) equipped with a ZORBAX Eclipse Plus C18 reversed-phase column (Agilent Technologies, Analytical 4.6×250mm 5-Micron) at 30 °C for quantifying total PET monomers released. The mobile phase was 0.1% formic acid in distilled water containing a 5-70% acetonitrile linear gradient over 20 min flowing at a rate of 0.8 ml min^{-1}. The effluent was monitored at a wavelength of 240 nm and the peak areas of terephthalic acid (TPA), mono(2-hydroxyethyl) terephthalate (MHET), and bis-2-(hydroxyethyl) terephthalate (BHET) were determined. The amounts of MHET and TPA were calculated based on standards with known concentrations. TPA was purchased from Sigma-Aldrich (CAS, 100-21-0) and MHET was prepared by enzymatic hydrolysis of BHET (Sigma-Aldrich, CAS, 959-26-2) following the protocol described in a previous report [2].

3.8 Molecular docking and Molecular Dynamics simulation

MD simulations were carried out for *Is*PETase^{WT} (PDB 5XG0) and the *Is*PETase$^{S92P/D157A}$ variant (PDB 8J17) using Gromacs 2022.3 [3]. The ligand 2PET was docked to the protein structures using Autodock vina [4], and ten independent poses were generated, and prepared for the following simulations. The *Is*PETase^{WT}, *Is*PETase$^{S92P/D157A}$, ten *Is*PETase^{WT}/2PET complexes, and ten *Is*PETase$^{S92P/D157A}$/2PET complexes, were placed in a box with a 0.8 nm margin and filled with tip3p water molecules [5] and underwent 2000 steepest descent energy minimization steps. Then the systems were equilibrated and run for 40 ns with a 2 fs time step using the NPT ensemble at a temperature of 298.15 K, under the Amber ff14sb force field [6], and each

simulation was replicated 5 times. The trajectory was viewed and analyzed with Gromacs tools, PyMOL Molecular Graphics System (www.pymol.org), and gmx_mmpbsa script (https://github.com/Jerkwin/gmxtools/tree/master/gmx_mmpbsa). The structures were grouped to determine the structurally similar clusters according to the conformations among the MD trajectories by utilizing the cluster tool in Gromacs using the gromos clustering algorithm with a C_α RMSD cutoff between 0.10 to 0.15 nm in steps of 0.01 nm.

3.9 Quantum Chemistry Calculation and Intermolecular interactions analyzation

The interactions among *Is*PETase^{WT}/ *Is*PETase$^{S92P/D157A}$ and 2PET were analyzed by quantum chemistry calculations performed by Gaussian 09C [7]. The molecular structures of the *Is*PETase/2PET and *Is*PETase^{WT}/2PET complexes were optimized with B3LYP functional [8] and 6-311G* [9] basis. Then the interactions between the molecules were analyzed by the independent gradient model based on the Hirshfeld partition (IGMH) method [10] using Multiwfn [11].

3.10 AFM

AFM was performed on a Bruker Dimension icon atomic force microscope in tapping mode. Images were recorded after a surface scan on an area of 50 × 50 μm^2. Image analysis, including histograms and surface roughness, was performed using NanoScope Analysis 3.00.

References:

1. X. Han, W. Liu, J. W. Huang, J. Ma, Y. Zheng, T. P. Ko, L. Xu, Y. S. Cheng, C. C. Chen and R. T. Guo, *Nat Commun*, 2017, **8**, 2106.
2. Q. Yin, S. You, J. Zhang, W. Qi and R. Su, *Bioresour Technol*, 2022, **364**, 128026.
3. M. J. Abraham, T. Murtola, R. Schulz, S. Páll, J. C. Smith, B. Hess and E. Lindahl, *SoftwareX*, 2015, **1-2**, 19-25.
4. O. Trott and A. J. Olson, *Journal of Computational Chemistry*, 2010, **31**, 455-461.
5. W. L. Jorgensen, J. Chandrasekhar, J. D. Madura, R. W. Impey and M. L. Klein, *The Journal of Chemical Physics*, 1983, **79**, 926-935.
6. J. A. Maier, C. Martinez, K. Kasavajhala, L. Wickstrom, K. E. Hauser and C. Simmerling, *Journal of Chemical Theory and Computation*, 2015, **11**, 3696-3713.
7. M. J. Frisch, G. W. Trucks, H. B. Schlegel, G. E. Scuseria, M. A. Robb, J. R. Cheeseman, G. Scalmani, V. Barone, G. A. Petersson, H. Nakatsuji, X. Li, M. Caricato, A. Marenich, J. Bloino, B. G. Janesko, R. Gomperts, B. Mennucci, H. P. Hratchian, J. V. Ortiz, A. F. Izmaylov, J. L. Sonnenberg, D. Williams-Young, F. Ding, F. Lipparini, F. Egidi, J. Goings, B. Peng, A. Petrone, T. Henderson, D. Ranasinghe, V. G. Zakrzewski, J. Gao, N. Rega, G. Zheng, W. Liang, M. Hada, M. Ehara, K. Toyota, R. Fukuda, J. Hasegawa, M. Ishida, T. Nakajima, Y. Honda, O. Kitao, H. Nakai, T. Vreven, K. Throssell, J. A. Montgomery Jr.,

J. E. Peralta, F. Ogliaro, M. Bearpark, J. J. Heyd, E. Brothers, K. N. Kudin, V. N. Staroverov, T. Keith, R. Kobayashi, J. Normand, K. Raghavachari, A. Rendell, J. C. Burant, S. S. Iyengar, J. Tomasi, M. Cossi, J. M. Millam, M. Klene, C. Adamo, R. Cammi, J. W. Ochterski, R. L. Martin, K. Morokuma, O. Farkas, J. B. Foresman and D. J. Fox, *Journal*, 2016.

8. P. J. Stephens, F. J. Devlin, C. F. Chabalowski and M. J. Frisch, *The Journal of physical chemistry*, 1994, **98**, 11623-11627.

9. Ditchfield and R., *Journal of Chemical Physics*, 1971, **54**, 724-728.

10. T. Lu and Q. X. Chen, *Journal of Computational Chemistry*, 2022, **43**, 539-555.

11. T. Lu and F. Chen, *J Comput Chem*, 2012, **33**, 580-592.